

Mitotic entry in the presence of DNA damage is a widespread property of aneuploidy in yeast.

Heidi M. Blank¹, Jason M. Sheltzer¹, Colleen M. Meehl¹ and Angelika Amon^{1*}.

¹Koch Institute for Integrative Cancer Research, Department of Biology, Howard Hughes Medical Institute, Massachusetts Institute of Technology, 76-543, Cambridge, MA 02138, USA.

* To whom correspondence should be addressed: angelika@mit.edu

Keywords: aneuploidy, DNA replication. DNA damage, DNA damage checkpoint pathway, yeast

ABSTRACT

Genetic instability is a hallmark of aneuploidy in budding and fission yeast. All aneuploid yeast strains analyzed to date harbor elevated levels of Rad52-GFP foci, a sign of DNA damage. Here we investigate how continuously elevated levels of DNA damage impact aneuploid cells. We show that Rad52-GFP foci form during S phase, consistent with the observation that DNA replication initiation and elongation are impaired in some aneuploid yeast strains. We furthermore find that although DNA damage is low in aneuploid cells, it nevertheless has dramatic consequences. Many aneuploid yeast strains adapt to DNA damage and undergo mitosis despite the presence of unrepaired DNA leading to cell death. Wild-type cells exposed to low levels of DNA damage exhibit a similar phenotype indicating that adaptation to low levels of unrepaired DNA is a general property of the cell's response to DNA damage. Our results indicate that by causing low levels of DNA damage, whole chromosome aneuploidies lead to DNA breaks that persist into mitosis. Such breaks are the substrate for translocations and deletions that are a hallmark of cancer.

Introduction

Changes in chromosome number, a condition known as aneuploidy, have a profound impact on the fitness of an organism. In humans, for example, all autosomal monosomies and most autosomal trisomies are lethal. The few trisomies that are viable lead to early childhood lethality (Trisomy 13 and 18) or developmental abnormalities and mental retardation (Trisomy 21; reviewed in Pfau and Amon, 2012). Aneuploidy is also a hallmark of cancer. It is estimated that between 75% - 90% of solid human tumors are aneuploid (Schvartzman et al., 2010; Holland and Cleveland, 2009).

Given the profound impact of the aneuploid condition on human health it is essential to understand how chromosome copy number alterations affect cellular and organismal physiology. Comprehensive whole genome gene expression and proteome analyses revealed that changes in gene copy number lead to a corresponding change in gene expression of approximately 80% of genes (Torres et al., 2007; Torres et al., 2010; Pavelka et al., 2010; Stinge et al., 2012; Dephoure et al., 2014). Studies in budding yeast showed that it is these changes in gene expression that are responsible for the phenotypes seen in aneuploid cells. Introduction of chromosome-size amounts of human or mouse DNA that exhibit little transcriptional and translational activity in yeast have, unlike duplicated yeast chromosomes, little or no effect on fitness (Torres et al., 2007).

The demonstration that changes in relative gene expression are the primary source of the adverse effects of aneuploidy on cells and organisms prompts the question whether the phenotypes that are observed in aneuploid organisms are due to changes in the gene dosage of a small number of specific genes or are caused by the sum of changes in gene expression of many genes that on their own have little or no effect on fitness. The answer appears to be that both effects contribute to the aneuploid condition. For example, duplication of the *APP* gene is thought to be responsible for the early onset of Alzheimer's-like pathologies observed in individuals with Down Syndrome (Rovelet-Lecrux, et al. 2006). However, aneuploid yeast and mammalian cells also share phenotypes, collectively called the aneuploidy-associated stresses that appear to be caused by concomitant changes in dosage of many genes (Torres et al. 2007; Williams et al. 2008; Tang et al. 2011). Aneuploidy impairs proliferation of budding yeast, fission yeast and mammalian cells, with a G1 delay being especially prominent (Niwa et al., 2006; Torres et al., 2007; Stinge et al., 2012; Thorburn et al., 2013; Baker et al., 2004; Li et al., 2009; Thompson and Compton, 2008; Williams et al., 2008). Whole chromosomal aneuploidies also lead to a transcriptional response. A gene expression signature similar to the environmental stress response (ESR; Gasch et al., 2000) in budding yeast has been observed in aneuploid budding and fission yeast strains, *Arabidopsis*, mouse and human cells (Torres et al., 2007; Sheltzer et al., 2012; Sheltzer, 2013). Lastly, aneuploid cells exhibit phenotypes characteristic of the disruption of protein homeostasis. Aneuploid yeast and mammalian cells harbor higher levels of protein aggregates and exhibit sensitivity to compounds that interfere with protein folding and turnover (Torres et al., 2007; Torres et al., 2010; Oromondia et al., 2012; Tang et al., 2011; Stinge et al., 2012; Donnelly et al., 2014).

Here we investigate the molecular basis of one consequence of aneuploidy – genome instability. We previously generated 13 budding yeast strains harboring an additional copy of one of the yeast chromosomes (henceforth disomes; Torres et al., 2007). These strains exhibit increased genomic instability compared to euploid control strains (Sheltzer et al., 2011). Genomic instability was also observed in budding yeast strains harboring multiple aneuploidies and in fission yeast indicating that genomic instability is a wide-spread consequence of the aneuploid condition (Sheltzer et al., 2011; Zhu et al., 2012). Analysis of individual disomes revealed that different chromosomal aneuploidies elicit different forms of genomic instability. Some disomes exhibited increased chromosome loss rates, others increased mutation rates or mitotic recombination. However, interestingly all aneuploid yeast strains analyzed to date harbor elevated levels of Rad52 foci, a sign of DNA damage and ongoing homologous recombination (Lisby et al., 2001). Why Rad52-GFP foci accumulate in aneuploid cells was not understood.

We find that Rad52-GFP foci form during S phase and persist for prolonged periods of time in aneuploid yeast strains, indicating that replication defects cause increased double strand break formation and/or DNA repair defects. Indeed, our studies show that DNA replication initiation and elongation are impaired in several disomic yeast strains. We further show that the degree of DNA damage that the disomic yeast strains experience is not high, but nevertheless has dramatic consequences. Many disomic yeast strain analyzed entered mitosis inappropriately in the presence of DNA damage. This mitosis in the presence of unrepaired DNA was preceded by a prolonged cell cycle arrest, demonstrating that the disomes initially respond to the DNA damage but then adapt and enter mitosis in the presence of DNA lesions. Wild-type cells exposed to low levels of DNA damage exhibit a similar phenotype indicating that adaptation to low levels

of unrepaired DNA is a general property of the way in which cells respond to DNA damage. The consequences are dramatic. Haploid yeast cells permanently cease to divide within the next 1 – 2 divisions. However, in diploid cells death may not always be the outcome of such an aberrant mitosis. It could lead to deletions and translocations. Thus, whole-chromosome aneuploidy could facilitate the generation of structural chromosomal abnormalities, another hallmark of cancer.

Results

Rad52-GFP foci form during S phase and persist in disomic yeast strains

We previously analyzed the localization of the recombination protein Rad52-GFP in seven disomic yeast strains (disomes IV, V, VIII, X, XI, XIV, and XV) and yeast strains harboring multiple chromosome gains or losses (Sheltzer et al., 2011). All aneuploid strains analyzed harbored a higher percentage of cells containing Rad52-GFP foci than euploid control cells. To investigate the molecular basis of this phenotype we first asked when during the cell cycle Rad52-GFP foci form in the various disomic yeast strains. To this end we followed Rad52-GFP focus formation by time-lapse microscopy in strains disomic for chromosome I, IV, V, VIII, X, XI, XIV, or XV using the CellASIC microfluidics system.

In the experimental set-up we used, nearly every cell of wild-type and disomic strains experienced DNA damage as judged by the appearance of at least one Rad52-focus in the nucleus (Figure 1A). This is presumably due to the continuous exposure to short-wavelength light. We found that Rad52-GFP foci appeared within a few frames of when a bud was first detected, and resolved before nuclear division (Figure 1A, 1B montage 1 arrowhead). However, Rad52-GFP foci persisted for longer periods of time in the disomes than in wild-type (Figure 1A, 1B, montage 2). Whereas most wild-type cells harbored Rad52-GFP foci for 0 – 120 minutes, a significant fraction of disomic cells contained Rad52-GFP foci for more than 135 minutes (135 – 225 minutes) and many arrested with persistent Rad52-GFP foci (> 225 minutes; Figure 1C). Our previous studies demonstrated that the Rad52-GFP foci seen in the aneuploid yeast strains indeed represent sites of double strand break (DSB) repair because disomes harboring a *RAD52* deletion and thus cannot repair DSBs spawn daughter cells that are inviable at an increased frequency (Sheltzer et al., 2011). Interestingly, the disomic yeast strains exhibited an additional abnormality. In all but one disome analyzed, Rad52-GFP foci were also observed in cells undergoing anaphase (Figure 1D), a phenotype indicative of DNA damage checkpoint failure or adaptation. We conclude that disomic yeast strains harbor higher levels of damaged DNA and undergo mitosis in the presence of Rad52-GFP foci.

DNA damage occurs during DNA replication in the disomes.

We first investigated why disomic yeast strains harbor higher levels of Rad52-GFP foci. To this end we assessed when during the cell cycle DNA damage occurs. Rad52-GFP foci appeared concomitantly with bud formation indicating that DNA was damaged during DNA replication. However, Rad52 requires cyclin-dependent kinase (CDK) activity to form repair foci (Huertas et al., 2008; Aylon et al., 2004; Ira et al., 2004). It was therefore possible that the Rad52-GFP foci accumulated at sites of damage that occurred during the preceding mitosis or G1. To address this possibility we examined Mre11 localization. Mre11 is part of the MRX complex which functions at an early step in the repair of DSBs and does not require CDK activity to associate with sites of DNA damage (reviewed in: Stracker and Petrini, 2011)

When wild-type cells are treated with the DNA damaging agent methyl methanesulfonate (MMS) Mre11-GFP foci are seen throughout the cell cycle (Figure 1E) indicating that Mre11-GFP can bind to DSBs in all cell cycle stages. In disomes I, V, VIII and XI Mre11-GFP foci appeared at the time of budding (Figure 1E). In a few cells, the focus was visible shortly before the appearance of the bud. We believe that this is unlikely to be a sign of DNA damage occurring during G1 but DNA damage occurring during very early stages of S phase in cells where the bud forms outside the plane of focus. Mre11-GFP foci appeared earlier than Rad52-GFP foci with respect to budding, which is consistent with the known residence time of these two proteins at DSBs (Stracker and Petrini, 2011). Because Mre11-GFP foci are rarely seen outside of S-phase in the disomes, we conclude that DNA damage occurs during DNA replication. The analysis of histone H2A phosphorylation supports this conclusion. Phosphorylation of histone H2A, a very early response to DNA damage was not detected in G1 arrested wild-type and disomic yeast strains (Supplemental Figure 1, 0 time point). However, all cells were capable of phosphorylating histone H2A when challenged with MMS during the G1 arrest (Supplemental Figure 1, 30 and 60 minute time points).

Disomes V and VIII exhibit DNA replication defects.

Our previous studies indicated that levels of Rad52-GFP foci or any other manifestations of genomic instability neither correlated with degree of aneuploidy nor any other phenotype shared between the disomic strains (Sheltzer et al., 2011). This observation prompted us to pursue the hypothesis that different disomic strains exhibit different defects in DNA replication and repair. Some disomic yeast strains could experience more DNA damage during S phase whereas others could have difficulties repairing the damaged DNA.

We first considered the possibility that DNA replication was impaired in some of the disomes causing increased formation of DSBs. To test this idea we analyzed DNA replication in disomes V and VIII because both strains are exquisitely sensitive to the DNA replication inhibitor hydroxyurea (HU; Sheltzer, et al., 2011). We synchronized cells in G1 with α -factor pheromone and monitored DNA replication following release from the G1 block. We included a strain lacking the gene encoding the S phase cyclin Clb5 in this analysis because *clb5 Δ* cells show both replication initiation and elongation defects (Epstein and Cross, 1992; Schwob and Nasmyth, 1993).

Most disomes exhibit delays in cell cycle entry due to defects in the G1 – S phase transition (Torres, et al., 2007; Thorburn et al., 2013). To distinguish these cell cycle entry defects from DNA replication initiation defects we designated the time point when DNA replication was first noticeable as the 0 time point and closely followed DNA replication for the next 50 minutes (Figure 2A). This analysis showed that cells disomic for chromosome V were both slow to initiate and complete DNA replication. Whereas the majority of wild-type cells had initiated DNA replication within 5 minutes of the first sign of DNA replication as judged by increased DNA content in the entire population (the entire distribution shifted to the right), only a small fraction of disome V cells had initiated DNA replication as judged by an extending of the DNA content distribution to the right (Figure 2A). This delay was especially obvious when comparing the 10 minute time points. Disome V cells were also slow to complete DNA replication. Whereas the majority of wild-type cells had completed DNA replication within 25 minutes of initiation replication was not completed until 35 minutes after initiation in disome V cells (Figure 2). This replication elongation defect is best seen when the replication profiles of the

later time points are superimposed (Figure 2B). We conclude that disome V cells exhibit replication initiation and elongation defects. These defects are subtle as judged by the fact that they are less pronounced than those of cells lacking *CLB5* (Figure 2A, B).

To further examine the kinetics of DNA replication initiation and elongation in disome V cells we pooled DNA samples from the start of replication until its completion and determined DNA copy number by deep sequencing. DNA copy number was assessed relative to a G1 sample (Figure 2C and Supplemental Figure 2). In this analysis regions of the genome that replicate early, such as origins of DNA replication, will appear as peaks whereas regions replicated late will appear as valleys (Yabuki et al., 2002). The DNA replication initiation and elongation defects of *clb5Δ* cells were readily observable in this analysis with peak height reduced and slopes less steep (Figure 2C and Supplemental Figure 2). Consistent with our DNA content analysis, the replication defect in disome V cells was less pronounced than that of cells lacking *CLB5*. However, decreased peak height and slope steepness were nevertheless evident in a significant fraction of the genome (Figure 2C and Supplemental Figure 2). We conducted this analysis from three biological replicates making us confident that the subtle replication defect that we observe is indeed a biological property of disome V cells rather than due to technical variability. We conclude that cells harboring an additional copy of chromosome V exhibit DNA replication initiation and elongation defects. We also observed earlier replication in a small number of regions of the genome in disome V cells (i.e. Figure 1C). Whether these few regions represent cryptic origins that are fired when replication proceeds slowly remains to be determined.

Like disome V, disome VIII exhibited a subtle DNA replication initiation defect (Figure 2A). However, once initiation had occurred replication elongation appeared to proceed efficiently (Figure 2A, B). The analysis of replication profiles substantiated this finding. Initiation of replication at some origins appeared delayed as judged by a decrease in peak height but alterations in slope, which are indicative of changes in replication elongation speed were not evident (Figure 2C, Supplemental Figure 2).

Subtle changes in replication could be due to changes in the balance between firing of origins in the rDNA and early origins. For example cells lacking the rDNA silencing factor Sir2 exhibit a delay in early origin firing (Yoshida et al., 2014). rDNA replication was not significantly altered in disome V and VIII cells (data now shown) indicating that alterations in rDNA replication were not responsible for the delay in early origin firing in the two disomes.

Replication initiation defects can be detected when comparing the frequency of loss of a plasmid carrying one origin of replication (ARS) with that of a plasmid carrying eight ARS sequences (Hogan and Koshland, 1992; Cheng et al., 2010). Indeed cells harboring a temperature sensitive allele in the gene encoding the replication initiation factor Cdc6 lose plasmids with a single ARS at a much higher frequency than plasmids with eight ARSs (Figure 3A; Hogan and Koshland, 1992). Disome V and VIII cells also exhibited an increased frequency in the loss of a single ARS plasmid that was suppressed when additional ARS sequences were present on the plasmid (Figure 3A, B). The degree of plasmid loss seen was similar to that of cells lacking *CLB5* (Figure 3B). We conclude that cells carrying an extra copy of chromosome V or VIII exhibit defects in DNA replication initiation. We note that disomes XI, XV and XVI also exhibit similar replication initiation defects in this assay (Supplemental Figure 3).

Genetic interactions between disome V and VIII and deletions in genes required for efficient DNA replication support the idea that the two disomes are defective in DNA replication. Tof1, Mrc1 and Csm3 function in a complex that associates with DNA polymerase during replication elongation and are thought to convey processivity to DNA polymerase and mediate DNA damage checkpoint surveillance (Bando et al., 2009; Tourriere et al., 2005; Hodgson et al., 2007). Deleting *MRC1* significantly enhanced the sensitivity of disome V and VIII to the DNA replication inhibitor hydroxyurea (HU) and the sensitivity of disome V cells to the DNA damaging agent phleomycin or MMS (Figure 3B; Sheltzer et al., 2011; note that disome VIII cells are so sensitive to phleomycin that it was not possible to detect enhancement at the phleomycin concentrations used in this analysis). The HU sensitivity of disome VIII cells was also enhanced by deleting *TOF1* (Figure 3C).

We observed similar genetic interactions between deletions of *TOF1* or *MRC1* and other disomes. Almost all disomes analyzed exhibited increased HU sensitivity when combined with a deletion in *MRC1* or *TOF1* and many showed increased sensitivity to phleomycin (Figure 3B, C). We conclude that disomes V and VIII are defective in DNA replication initiation. As judged by the genetic interactions with *mrc1Δ* or *tof1Δ* and plasmid loss assays this defect is not restricted to these two disomes but is a widespread phenomenon among the disomic yeast strains. Disome V cells also exhibit replication elongation defects. Whether this is a common occurrence among the disomes remains to be determined.

Repair of an HO-induced double strand break is normal in disomes I, V, VIII, X and XI.

The extended presence of Rad52-GFP foci in some of the disomic strains could be due to defects in repair of damaged DNA. To test this possibility, we introduced a galactose-inducible HO endonuclease construct into euploid and some disomic yeast strains. HO's only target site in the yeast genome is within the MAT locus. Cleavage in the MAT locus facilitates mating type conversion. Using appropriate restriction enzymes, HO cleavage and repair of the HO induced DSB from the silent mating type locus encoding the opposite mating type can be followed over time by Southern blot analysis (reviewed in Sugawara and Haber, 2006).

We added galactose to exponentially growing cells for 40 minutes, which led to efficient cleavage in the mating type locus (*MATa* cut; Figure 4A). Upon repression of HO expression by glucose addition, the double strand break was efficiently repaired from the silent *HMLα* locus, as judged by the appearance of the recombinant product termed *HMLα* (Figure 4A). The kinetics of repair in disomes V, VIII and XI were indistinguishable from that of the wild-type strain (Figure 4A). We should note that the disome V strain harboring the *GAL-HO* construct was for unknown reasons unstable. Only 80% of cells harbored the additional copy of chromosome V despite continuous selection for the extra chromosome (Supplemental Figure 4).

Given that the increase in Rad52-GFP focus formation was subtle in many of the disomes we hypothesized that the disomes are capable of efficiently repairing minor DNA damage, such as a single HO-induced DSB, but may have difficulties repairing a HO break in the presence of high levels of DNA damage. To test this hypothesis we examined the repair kinetics of the HO-induced break in the *MATa* locus in the presence of 10μg/mL phleomycin, either 1 hour prior to repair (Figure 4B, top panel) or 1 hour prior

and during repair (Figure 4B, middle and bottom panel). We analyzed disomes I, V, VIII, X and XI using this experimental strategy and found all disomes to repair the HO break efficiently (Figure 4B). We conclude that repair of an endonuclease-induced DSB is not affected in disomes I, V, VIII, X and XI. However, it is important to note that this finding does not exclude the possibility that the disomes have difficulty repairing other types of DNA damage. In fact, the finding that the disomes are sensitive to DNA damaging agents strongly argues that chemically-induced DNA damage that could involve combinations of complex DNA breaks, cross links and adducts are not effectively repaired in the disomes.

Disomic yeast strains undergo mitosis in the presence of DNA damage.

The live-cell analysis described in Figure 1 showed that in addition to harboring Rad52-GFP foci that persist longer in cells, many disomes entered anaphase in their presence. This observation raised the interesting possibility that these disomic yeast strains either fail to recognize damaged DNA or adapt to the damage and enter mitosis without having repaired the damage.

In response to DNA damage cells activate the DNA damage checkpoint, which in turn halts cell cycle progression prior to entry into mitosis in mammals and the onset of anaphase in budding yeast (reviewed in Zhou and Elledge, 2000). Our previous studies showed that the DNA damage response was functional in the disomic yeast strains as judged by the ability of the disomic strains to activate the DNA damage checkpoint kinase Rad53 in response to treatment of cells with the DNA damaging agent phleomycin (Sheltzer et al., 2011). However, the amount of damage caused by this treatment is high. We therefore considered the possibility that the low degree of DNA damage generated in the disomic yeast strains was insufficient to generate a robust DNA damage response and cell cycle arrest. To test this hypothesis we determined whether cells arrested prior to mitosis before initiating anaphase with a Rad52-GFP focus. This analysis revealed that the disomes arrested for long periods of time during which a Rad52-GFP focus was continuously present before finally entering anaphase in the presence of a Rad52-GFP focus (Figure 5A; disome I: 276 minutes, disome II: 306 minutes, disome V: 261 minutes, disome VIII: 346 minutes, disome X: 345 minutes, disome XI: 270 minutes, disome XIV: 344 minutes, disome XV: 265 minutes). Thus, the disomes initially respond to the DNA damage but eventually enter mitosis despite the presence of a Rad52-GFP focus.

Is entry into anaphase in the presence of Rad52-GFP foci a characteristic of the disomic yeast strains or a more general property of cells responding to low levels of DNA damage? To address this question we treated wild-type cells with increasing doses of MMS. This analysis revealed that at doses between 0.04 – 0.08% MMS as many as 40 percent of wild-type cells underwent anaphase despite the presence of a Rad52-GFP focus (Figure 5B). At higher MMS concentrations, cells permanently arrested in metaphase. Like in the disomes, anaphase entry in the presence of a Rad52 focus was preceded by a prolonged cell cycle arrest (211 minutes) during which time a Rad52-GFP focus was continuously present (Figure 5A). It thus appears that wild-type cells, too, detect low levels of DNA damage, arrest prior to anaphase for significant periods of time but eventually segregate their chromosomes despite not having resolved Rad52-GFP foci.

Before concluding that low levels of DNA damage may not be an absolute barrier to anaphase entry, it was important to establish that the Rad52 foci observed in cells

undergoing anaphase indeed represented DNA damage and were not simply Rad52-GFP remnants on successfully repaired DNA. To address this possibility we followed the fate of wild-type cells challenged with low doses of MMS that had undergone mitosis despite harboring a Rad52-GFP focus. This analysis revealed that only 4% of cells continued to divide without any apparent defect (Figure 5C). All other cells showed significant proliferation defects following the anaphase during which a Rad52-GFP focus was present. 75% of such cells arrested in the subsequent cell cycle (Figure 5C). The remaining 21% proceeded through one additional division and then did not divide within the time frame of the movie (Figure 5C). This analysis demonstrates that the presence of a Rad52-GFP focus during anaphase indeed reflects mitosis occurring in the presence of unrepaired DNA with dramatic detrimental consequences for the cell. We conclude that when low-levels of DNA damage are not successfully repaired within 4 – 6 hours, cells adapt and proceed through mitosis in the presence of damaged DNA. Adaptation occurred faster in our experimental setup than in previous studies where a single DSB was generated during G1 when a repair template is absent. Under these conditions cells arrested for 8 hours or more before entering mitosis in the presence of this double strand break (Pellicioli et al., 2001). We do not know why adaptation occurs more quickly in our experimental setup but speculate that it is due to differences in the nature of the DNA damage. A single DSB created during G1 could generate long tracks of resected single stranded DNA that emit a strong and persistent DNA damage checkpoint signal. The DNA damage elicited by MMS in wild-type cells or by fork collapse in the disomes may generate a weaker or more short-lived checkpoint signal.

Discussion

Genetic instability is a hallmark of aneuploidy in budding and fission yeast. Every aneuploid yeast strain we and others have analyzed to date exhibits some form of genomic instability. Chromosome loss rate, mutation rate as well as microsatellite instability were observed in many different yeast strains harboring single additional chromosomes. A very prominent phenotype among aneuploid budding and fission yeast strains is an increase in the percentage of cells harboring Rad52-GFP foci. Here we investigate the molecular basis of this phenotype. We find that Rad52-GFP foci form during S phase, indicating that replication defects cause increased double strand break formation. The levels of DNA damage that the disomic strains experience are not high, but they have a significant impact on cellular fitness. Many disomic yeast strain enter mitosis in the presence of DNA damage following a prolonged cell cycle arrest. Wild-type cells exposed to low levels of DNA damage exhibit a similar phenotype indicating that adaptation to low levels of DNA damage is a general property of the manner in which cells respond to DNA damage. If genomic instability is also a property of aneuploid mammalian cells this aspect of the DNA damage response could very well contribute to the structural abnormalities that are so frequently observed in cancer.

In our live-cell analysis wild-type and aneuploid yeast strains accumulated Rad52-GFP foci during S phase, but they persisted for longer periods of time in the aneuploid strains. We did not detect DNA damage repair defects in the disomes that we analyzed, but DNA replication initiation and elongation defects were detected in many disomic yeast strains. From these results we conclude that an increased number of DSBs contributes to the prolonged presence of Rad52-GFP foci in the disomic strains. Determining how many more DSBs form in disomic strains than wild-type was however not possible because Rad52-GFP foci cluster within cells (Lisby et al, 2001).

A detailed analysis of disomes V and VIII revealed replication initiation problems in both strains and replication elongation defects in disome V cells. It thus appears that various aspects of DNA replication are sensitive to aneuploidy. Why DNA replication is affected by so many different aneuploidies is not clear. Chromatin structure as well as DNA replication initiation and elongation are mediated by many large multi-subunit complexes. Stoichiometric imbalances in one or several of the complexes required for error-free DNA replication could arise in many different aneuploidies. This in turn could cause the formation of partially assembled complexes or interfere with the function of these complexes in some other manner. Thus far, we have not been able to identify the genes that cause the DNA replication defects in the different disomes. We screened through a centromere-based plasmid library that harbors 75% of the genes encoded on chromosome VIII but were not able to identify a single gene, which when introduced in single copy into wild-type cells confers hydroxyurea or phleomycin sensitivity (H. B., unpublished observations). It thus appears that changes in copy number of multiple genes on chromosome 8 are responsible for the sensitivity to genotoxic agents and presumably the DNA replication defects that are observed in disome VIII cells.

While replication defects appear wide-spread among the disomes, we have thus far not obtained any evidence to indicate that DSB repair is impaired in the disomes. Repair of an HO-induced DSB occurred with wild-type kinetics in all the disomic strains we analyzed irrespective of whether it was the only DNA damage that was induced or whether it was generated in the context of additional genotoxin-induced DNA damage. However this result does not necessarily mean that these disomic yeast strains can repair all forms of DNA damage effectively. The fact that most aneuploid yeast strains are sensitive to DNA damaging agents such as phleomycin or MMS in fact strongly argues that some forms of chemically-induced DNA damage are not repaired efficiently in the disomes. Further studies are needed to determine the identity of this DNA damage.

The perhaps most striking phenotype we observed is that a fraction of disome I, II, V, VIII, XIV, and XV cells entered mitosis despite the presence of DNA damage. The percentage of cells entering anaphase in the presence of a Rad52-GFP focus was also elevated in disomes X and XI but did not reach significance. Disome IV cells never entered anaphase despite harboring a Rad52-GFP focus. Disome IV cells proliferate extremely poorly (Torres et al., 2007) which could account for the fact that entry into mitosis in the presence of DNA damage does not occur. Wild-type cells treated with low doses of the DNA damaging agent MMS also progressed through mitosis with Rad52-GFP foci.

Our live-cell imaging analysis showed that cells initially arrested in metaphase but eventually adapted and then entered anaphase without having repaired their damaged DNA. Adaptation to DNA damage has been proposed to serve as a last-ditch effort at survival after all repair options have been exhausted (Vidanes et al., 2010). However, in haploid cells this effort is largely futile. The vast majority of cells that underwent anaphase with a Rad52-GFP focus ceased to divide within 1 - 2 cell divisions. It is however worth noting that adaptation in the presence of low-levels of DNA damage may provide a survival benefit in diploid cells. The presence of two chromosomal copies likely protects cells from dying even when significant amounts of genetic information are lost as the result of chromosome segregation in the face of unrepaired DSBs. Thus, it will be very interesting to uncover the molecular mechanisms that either quench DNA damage signaling or override it to mediate adaptation. The Polo kinase Cdc5 has been

shown to be required for adaptation to DNA damage in yeast and mammals (Toczyski et al., 1997; Pellicoli et al., 2001; Yoo et al., 2004; reviewed in Serrano and D'Amours, 2014). Cdc5 down-regulates the DNA damage checkpoint pathway through inhibiting the DNA damage checkpoint kinase Rad53 (Vidanes et al., 2010; reviewed in Serrano and D'Amours, 2014). Determining whether the kinase responds differently to low and high levels of DNA damage will be important questions in the future.

Our findings raise the remarkable possibility that in multicellular organisms low levels of DNA damage may in fact be more detrimental than high levels of damage. Mitosis in the presence of DNA damage can lead to translocations, deletions and other types of mutagenic events. As such genomic alterations have all been implicated in tumorigenesis, low levels of DNA damage could have substantial pro-tumorigenic effects. Given that mitosis in the presence of DNA damage is a key characteristic of aneuploidy, it is furthermore tempting to speculate that this aspect of aneuploidy could contribute to tumor evolution thus explaining why the aneuploid condition, despite its anti-proliferative effects is a hallmark of cancer.

Materials and Methods:

Strains and plasmids:

Strains used in this study are described in Supplemental Table1 and are derivatives of W303. Strains were constructed using PCR-based methods described by Longtine et al. (Longtine et al. 1998). The generation of disomic strains has been described previously (Torres et al. 2007). Karyotypes of all disomic strains were confirmed by comparative genome hybridization (Torres et al. 2007). Growth conditions are described in the figure legends.

Live cell microscopy

Cells harboring a GFP-tagged copy of *RAD52* at the endogenous locus were grown to log phase in SC-HIS+G418 medium and transferred to a microfluidic chamber (CellASIC Corp. Hayward, CA). Cells were imaged every 15 minutes using a Zeiss Axio Observer-Z1 with a 100X objective, equipped with a Hamamatsu ORCA-ER digital camera. 11 Z-stacks (0.6 microns apart), 100 msec exposure, full gain, 2x2 binning, were acquired and maximally projected. A single transmitted light 20 msec exposure image was acquired for each Z-stack. Metamorph software was used for image acquisition and processing.

For MMS treatment and imaging, cells were grown overnight in SC-HIS+G418 medium, then transferred to YPD and arrested with α -factor for ~ 105 min. MMS was added at the indicated concentration for approximately 25 minutes while cells were still arrested in G1. Cells were then washed and transferred to fresh selective medium lacking pheromone and imaged on a microfluidic chamber as above.

Cells harboring a GFP-tagged copy of *MRE11* at the endogenous locus were imaged similarly to cells carrying a tagged copy of *RAD52*, but instead of a microfluidic chamber, cells were placed on an agarose pad slide and imaged every 7.5 minutes. Additionally, we employed Definite Focus (Zeiss) to ensure images remained in focus.

For Figures 1A and 1C, only cells that had a foci and divided in 25 or less time frames were included in our analysis. The analysis in Figure 1D included only the first division following release from the G1 arrest to avoid artifacts caused by cells experiencing DNA

damage due to imaging them for varying lengths of time.

DNA copy number analysis

DNA was extracted according to Blitzblau et al. (2012).

Samples were sequenced on an Illumina HiSeq to produce paired end reads 40nt in length. Reads were aligned to the W303 genome and processed with module add bwa version 0.7.5a, samtools version 0.1.19, bedtools version 2.17.0 and ucsc-tools version 20120530. Alignment data were expressed as counts of first in pair reads from properly aligned pairs (sam flags 99 and 83) with mapping quality 10 or better per 50 base pair window per 5 million accepted reads.

For each strain the number of counts for each replicate was summed and then divided by the G1 count values corresponding to that strain. (For example, $(WTa+WTb+WTc)/WT_{G1}$.) For the *clb5Δ* strain, the WT G1 count values were used for normalization. A loess smoothing function was performed on each chromosome, where span was equal to $0.025 \times \max(\text{largest chromosome length} / \text{chromosome } x \text{ length})$, where chromosome x is the length of the chromosome of interest. This normalized the amount of smoothing to the size of each particular chromosome. A loess.predict command was then used to give values for any data that were missing. The loess.predict values versus chromosome position were plotted.

Mating type switching time courses

Time courses were carried out as described in Hicks et al. (2011). Briefly, cells were grown in YP-lactate. 2% galactose was added (0 time point) to induce *HO* expression. 40 minutes thereafter *HO* expression was repressed by the addition of 2% glucose. For time courses involving the addition of phleomycin, cells were re-suspended in YP-lactate buffered with 50mM HEPES, pH 7.4. Phleomycin was added to a final concentration of 10 $\mu\text{g/mL}$ for 60 minutes prior to the addition of galactose, and either washed out before repair or left in the medium for the remainder of the experiment as indicated in the text.

Genomic DNA was isolated at the indicated time points and digested with *Styl*. DNA was separated on a 1% agarose gel made in 1X TBE, run in 1X TBE buffer at 150V. Neutral transfer to the membrane (GE Healthcare Amersham Hybond-N+) was carried out according to the manufacturer's protocol using a basic capillary transfer apparatus using 20X SSC as transfer buffer. Following overnight transfer, the membrane was cross-linked using the pre-set UV exposure on a GE Healthcare UVC 500 cross-linker (70,000 micro-Joules/cm²).

The ³²P labeled probe was the PCR product of primers AW264 and MAT10, described in Hicks et al. (2011) using the Megaprime DNA Labeling System and ProbeQuant G-50 Micro Columns (Amersham). The blot was exposed to a storage phosphor screen and imaged using a Typhoon Trio (Amersham). The *HMLα* fragment served as loading control for the experiment, as the concentration remains unchanged throughout the time course.

γ -H2A immunoblot analysis.

Strains were grown overnight in SC-HIS+G418 medium and transferred to YPD at $OD_{600nm} \approx 0.18$. Cells were arrested in G1 with α -factor (5 $\mu\text{g/mL}$) for the duration of the

experiment. 160 minutes into arrest MMS (0.3%) was added. Samples were collected before MMS addition and at the indicated time points.

Protein samples were TCA extracted as described in Attner and Amon (2012) and separated by PAGE, 15% acrylamide gel, and transferred onto a nitrocellulose membrane. The membrane was blocked in 5% BSA in TBST for 30 minutes. γ -H2A was detected by incubation with the primary antibody (Abcam rabbit polyclonal 15083) at 1:1000 in blocking buffer at RT for one hour, followed by washing and incubation with the secondary antibody anti-rabbit HRP at 1:10,000 in blocking buffer at RT for 40 minutes. α -Pgk1 antibodies (Molecular Probes) were used at a 1:10,000 dilution.

Flow cytometry

Cells were re-suspended in 70% ethanol. After fixation, cells were washed once and resuspended in 50mM sodium citrate, pH 7.0, containing 0.25 mg/mL of RNase A. Samples were incubated at 37°C overnight. Samples were then pelleted and resuspended in 50mM sodium citrate containing 1 μ M Sytox Green (Lifetechnologies). Cells were kept in the dark for at least one hour and sonicated prior to analysis on the flow cytometer model BD FACSCalibur™ running CellQuest Pro software.

Plasmid loss experiments

The loss rates of plasmids harboring 1 or 8 ARS sequences, as well as a selectable *LEU2* marker, were determined as described in Zhang et al. (2002). In brief, cells were first grown overnight in –HIS-LEU+G418 medium. Subsequently, 200 cells were plated on –HIS+G418 plates and 200,000 cells were inoculated into –HIS+G418 medium and allowed to grow for an additional 24 hours. After this time, 200 cells were plated on –HIS+G418 plates. After 3-5 days of growth, the –HIS+G418 plates were replica plated to –HIS-LEU+G418 plates to determine the fraction of cells that had lost the plasmid. In the experiment shown in Figure 3A and Supplemental Figure 3, 12 biological replicates were analyzed; in the experiment shown in Figure 3B, 3 biological replicates were analyzed.

Acknowledgments:

We thank Steve Bell for the *cdc6-1* mutant strain, Jim Haber for the *GAL-HO* construct, and Chun Liang for the p1ARS and p8ARSs plasmids. We thank Charlie Whittaker of The Barbara K. Ostrom (1978) Bioinformatics and Computing Facility in the Swanson Biotechnology Center and Theresa and Clara Weis for technical support. We thank members of the Amon Lab for suggestions. This work was supported by the National Institute of Health (GM056800 to A.A), a Ruth L. Kirschstein NRSA Fellowship to H. B. and National Science Foundation Graduate Fellowship to J. S. This work was supported in part by the Koch Institute Support (core) Grant P30-CA14051 from the National Cancer Institute. A.A is an investigator of the Howard Hughes Medical Institute.

References:

Attner MA, Amon A (2012). Control of the mitotic exit network during meiosis. *Mol Biol Cell* 16, 3122-3132.

Aylon Y, Liefshitz B, Kupiec M (2004). The CDK regulates repair of double-strand breaks by homologous recombination during the cell cycle. *EMBO J.* 23, 4868–4875.

Baker DJ, Jeganathan KB, Cameron JD, Thompson M, Juneja S, Kopecka A, Kumar R, Jenkins RB, de Groen PC, Roche P, van Deursen JM (2004). BubR1 insufficiency causes early onset of aging-associated phenotypes and infertility in mice. *Nat Genet.* 36, 744-749.

Bando M, Katou Y, Komata M, Tanaka H, Itoh T, Sutani T, Shirahige K (2009). Csm3, Tof1, and Mrc1 form a heterotrimeric mediator complex that associates with DNA replication forks. *J Biol Chem* 284, 34355–34365.

Blitzblau HG, Chan CS, Hochwagen A, Bell SP (2012). Separation of DNA replication from the assembly of break-competent meiotic chromosomes. *PLoS Genet* 8, e1002643.

Cheng X, Xu Z, Wang J, Zhai Y, Lu Y, Liang C (2010). ATP-dependent pre-replicative complex assembly is facilitated by Adk1p in budding yeast. *J Biol Chem* 285, 29974-29980.

Dephoure N, Hwang S, O'Sullivan C, Dodgson SE, Gygi SP, Amon A, Torres EM (2014). Quantitative proteomic analysis reveals posttranslational responses to aneuploidy in yeast. *eLife* 3, e03023.

Donnelly N, Passerini V, Durrbaum M, Stingle S, Storchova Z (2014). HSF1 deficiency and impaired HSP90-dependent protein folding are hallmarks of aneuploid human cells. *Embo J pii*, e201488648

Epstein CB, Cross FR (1992). CLB5: a novel B cyclin from budding yeast with a role in S phase. *Genes Dev* 6, 1695-1706.

Gasch AP, Spellman PT, Kao CM, Carmel-Harel O, Eisen MB, Storz G, Botstein D, Brown PO (2000). Genomic expression programs in the response of yeast cells to environmental changes. *Mol Biol Cell* 11, 4241-4257.

Hicks WM, Yamaguchi M, Haber JE (2011). Real-time analysis of double-strand DNA break repair by homologous recombination. *Proc Natl Acad Sci U S A* 108, 3108-3115.

Hodgson B, Calzada A, Labib K (2007). Mrc1 and Tof1 regulate DNA replication forks in different ways during normal S phase. *Mol Biol Cell* 18, 3894–3902.

Hogan E, Koshland D (1992). Addition of extra origins of replication to a minichromosome suppresses its mitotic loss in *cdc6* and *cdc14* mutants of *Saccharomyces cerevisiae*. *Proc Natl Acad Sci U S A* 89, 3098-3102.

Holland AJ, Cleveland DW (2009). Boveri revisited: chromosomal instability, aneuploidy and tumorigenesis. *Nat Rev Mol Cell Biol* 10, 478–487.

Huertas P, Cortés-Ledesma F, Sartori AA, Aguilera A, Jackson SP (2008). CDK targets Sae2 to control DNA-end resection and homologous recombination. *Nature* 455, 689-692.

- Ira G, et al. (2003). DNA end resection, homologous recombination and DNA damage checkpoint activation require CDK1. *Nature* 431, 1011–1017.
- Li M, Fang X, Wei Z, York JP, Zhang P (2009). Loss of spindle assembly checkpoint-mediated inhibition of Cdc20 promotes tumorigenesis in mice. *J Cell Biol* 185, 983-994.
- Lisby M, Rothstein R, Mortensen UH (2001). Rad52 forms DNA repair and recombination centers during S phase. *Proc Natl Acad Sci U S A* 98, 8276-8282.
- Longtine MS, Fares H, Pringle JR (1998). Role of the yeast Gin4p protein kinase in septin assembly and the relationship between septin assembly and septin function. *J Cell Biol* 143, 719-736.
- Niwa O, Tange Y, Kurabayashi A (2006). Growth arrest and chromosome instability in aneuploid yeast. *Yeast* 23, 937–950.
- Oromendia AB, Dodgson SE, Amon A (2012). Aneuploidy causes proteotoxic stress in yeast. *Genes & Development* 26, 2696–2708.
- Pavelka N, Rancati G, Zhu J, Bradford WD, Saraf A, Florens L, Sanderson BW, Hattem GL, Li R (2010). Aneuploidy confers quantitative proteome changes and phenotypic variation in budding yeast. *Nature* 468, 321–325.
- Pellicioli A, Lee SE, Lucca C, Foiani M, Haber JE (2001). Regulation of *Saccharomyces* Rad53 checkpoint kinase during adaptation from DNA damage-induced G2/M arrest. *Mol Cell* 7, 293-300.
- Pfau SJ, Amon A (2012). Chromosomal instability and aneuploidy in cancer: from yeast to man. *EMBO Rep* 13, 515-527.
- Rovelet-Lecrux, A, et al (2006). APP locus duplication causes autosomal dominant early-onset Alzheimer disease with cerebral amyloid antipathy. *Nat Genetics* 38, 24-26.
- Schvartzman J-M, Sotillo R, Benezra R (2010). Mitotic chromosomal instability and cancer: mouse modelling of the human disease. *Nat Rev Cancer* 10, 102–115.
- Schwob E, Nasmyth K (1993). CLB5 and CLB6, a new pair of B cyclins involved in DNA replication in *Saccharomyces cerevisiae*. *Genes Dev* 7, 1160-1175.
- Serrano D, D'Amours D (2014). When genome integrity and cell cycle decisions collide: roles of polo kinases in cellular adaptation to DNA damage. *Syst Synth Biol.* 8, 195-203.
- Sheltzer JM, Amon A (2011). The aneuploidy paradox: costs and benefits of an incorrect karyotype. *Trends Genet* 27, 446-453.
- Sheltzer JM, Torres EM, Dunham MJ, Amon A (2012). Transcriptional consequences of aneuploidy. *Proceedings of the National Academy of Sciences* 109, 12644–12649.

- Sheltzer JM. (2013). A transcriptional and metabolic signature of primary aneuploidy is present in chromosomally unstable cancer cells and informs clinical prognosis. *Cancer Res.* 73:6401-6412.
- Stingele S, Stoehr G, Peplowska K, Cox JUR, Mann M, Storchova Z (2012). Global analysis of genome, transcriptome and proteome reveals the response to aneuploidy in human cells. *Mol Syst Biol* 8, 1–12.
- Stracker TH, Petrini JH (2011). The MRE11 complex: starting from the ends. *Nat Rev Mol Cell Biol.* 12, 90-103.
- Sugawara N, Haber JE (2006). Repair of DNA double strand breaks: in vivo biochemistry. *Methods Enzymol* 408, 416-429.
- Thompson SL, Compton DA (2010). Proliferation of aneuploid human cells is limited by a p53-dependent mechanism. *J Cell Biol* 188, 369–381.
- Thorburn RR, Gonzalez C, Brar GA, Christen S, Carlile TM, Ingolia NT, Sauer U, Weissman JS, Amon A (2013). Aneuploid yeast strains exhibit defects in cell growth and passage through START. *Mol Biol Cell* 24, 1274–1289.
- Tang Y-C, Williams BR, Siegel JJ, Amon A (2011). Identification of Aneuploidy-Selective Antiproliferation Compounds. *Cell* 144, 499–512.
- Toczyski DP, Galgoczy DJ, Hartwell LH (1997). CDC5 and CKII control adaptation to the yeast DNA damage checkpoint. *Cell* 90,1097-1106.
- Torres EM, Dephoure N, Panneerselvam A, Tucker CM, Whittaker CA, Gygi SP, Dunham MJ, Amon A (2010). Identification of Aneuploidy-Tolerating Mutations. *Cell* 143, 71–83.
- Torres EM, Sokolsky T, Tucker CM, Chan LY, Boselli M, Dunham MJ, Amon, A (2007). Effects of aneuploidy on cellular physiology and cell division in haploid yeast. *Science* 317, 916–924.
- Tourrière H, Versini G, Cordon-Preciado V, Alabert C, Pasero P (2005). Mrc1 and Tof1 promote replication fork progression and recovery independently of Rad53. *Mol Cell* 19, 699–706.
- Vidanes GM, Sweeney FD, Galicia S, Cheung S, Doyle JP, Durocher D, Toczyski DP (2010). CDC5 inhibits the hyperphosphorylation of the checkpoint kinase Rad53, leading to checkpoint adaptation. *PLoS Biol* 8, e1000286.
- Williams BR, Prabhu VR, Hunter KE, Glazier CM, Whittaker CA, Housman DE, Amon A (2008). Aneuploidy affects proliferation and spontaneous immortalization in mammalian cells. *Science* 322, 703–709.
- Yabuki N, Terashima H, Kitada K (2002). Mapping of early firing origins on a replication profile of budding yeast. *Genes Cells* 7, 781–789.

Yoshida K, Bacal J, Desmarais D, Padioleau I, Tsaponina O, Chabes A, Pantescio V, Dubois E, Parrinello H, Skrzypczak M, Ginalska K, Lengronne A, Pasero P. (2014). The histone deacetylases sir2 and rpd3 act on ribosomal DNA to control the replication program in budding yeast. *Mol. Cell* 54, 691-697.

Yoo HY, Kumagai A, Shevchenko A, Shevchenko A, Dunphy WG (2004). Adaptation of a DNA replication checkpoint response depends upon inactivation of Claspin by the Polo-like kinase. *Cell* 117, 575-588.

Zhang Y, Yu Z, Fu X, Liang C. (2002). Noc3p, a bHLH protein, plays an integral role in the initiation of DNA replication in budding yeast. *Cell* 109, 849-860.

Zhou BB, Elledge SJ (2000). The DNA damage response: putting checkpoints in perspective. *Nature* 408, 433-439.

Zhu J, Pavelka N, Bradford WD, Rancati G, Li R (2012). Karyotypic Determinants of Chromosome Instability in Aneuploid Budding Yeast. *PLoS Genet* 8, e1002719.

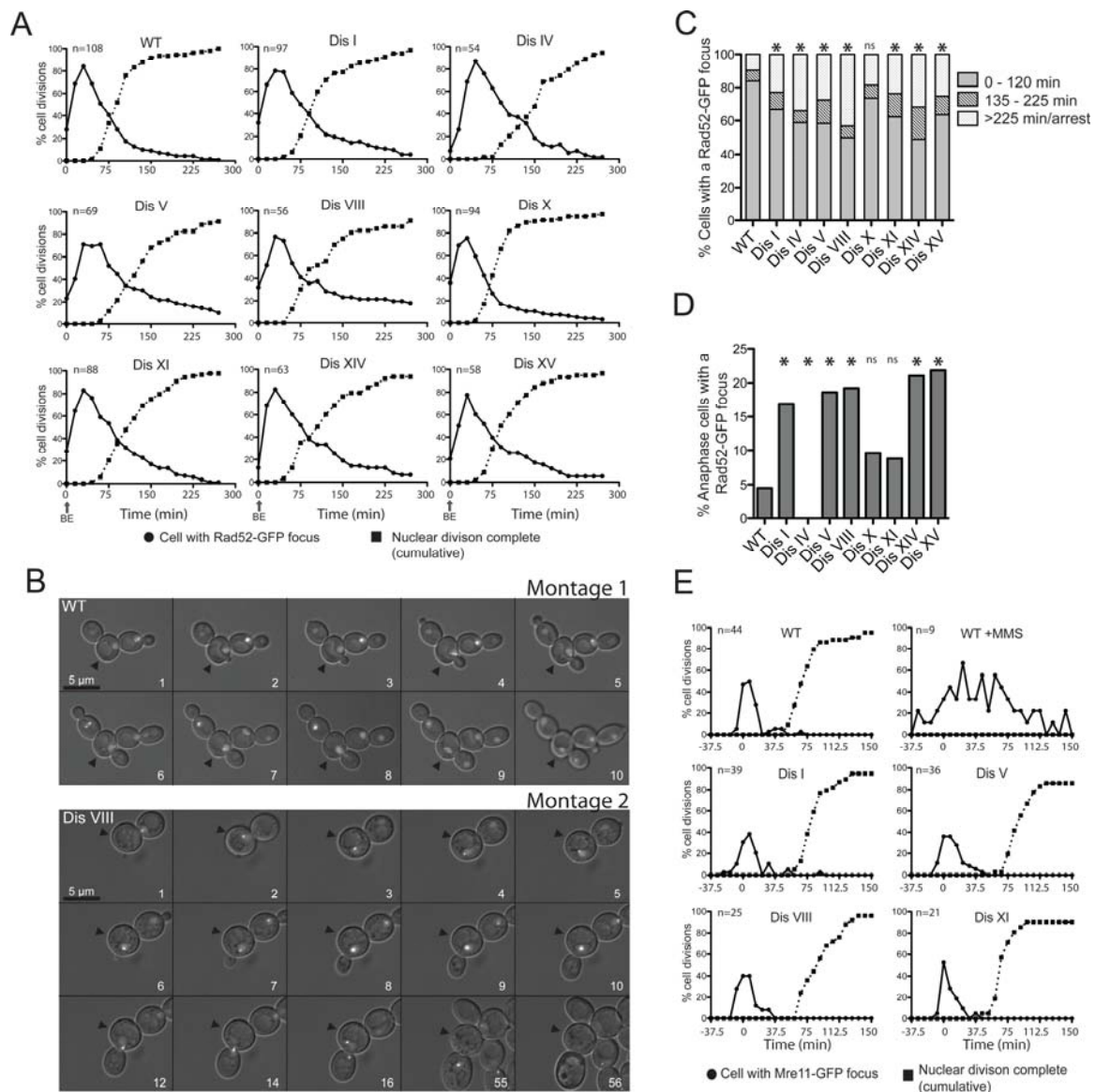


Figure 1. DNA damage incurs during S phase and can persist into anaphase in aneuploid yeast strains.

(A) Wild-type (A24352), disome I (A35868), disome IV (A26532), disome V (A26533), disome VIII (A25342), disome X (A25343), disome XI (A25421), disome XIV (A25344) and disome XV (A25345) cells containing a *RAD52-GFP* fusion were analyzed using time-lapse microscopy to analyze cellular morphology and the presence of Rad52-GFP foci in cells. The graphs show percent of cells that contain one or more Rad52-GFP foci (closed circles) or cumulative cell divisions (closed squares) over time. Cell divisions were synchronized so that the time of bud emergence (BE) occurred at the zero time point.

(B) Montage 1: Example of a wild-type cell (black arrowhead) acquiring a Rad52-GFP focus during S phase and resolving it prior to undergoing anaphase. A Rad52-GFP focus

was considered to be present in frames 3 – 9. The focus is weakly present in frame 3 and seen in the bud in frame 9.

Montage 2: Example of a disome VIII cell (arrowhead) acquiring a Rad52-GFP focus during S phase and undergoing anaphase in the presence of a Rad52-GFP focus. The cell subsequently dies. A Rad52-GFP focus was considered to be present in all frames except frame 56.

(C) Shows the percentage of cells analyzed in (A) harboring a Rad52-GFP focus for the indicated time brackets. WT n=136; Disome 1 n=144; Disome IV n=85; Disome V n=120; Disome VIII n=102; Disome X n=140; Disome XI n=114; Disome XIV n=104; Disome XV n=107. The asterisk above the column indicates statistical significance (Chi-square test; $p < 0.005$). ns indicates no statistically significant difference between wild type and disome X.

(D) Percentage of cells analyzed in (A) that proceed aberrantly into anaphase despite the presence of a Rad52-GFP focus. WT n=192; Disome 1 n=126; Disome IV n=85; Disome V n=93; Disome VIII n=80; Disome X n=123; Disome XI n=102; Disome XIV n=85; Disome XV n=81. The asterisk above the column indicates statistical significance (Chi-square test; $p < 0.05$). ns indicates no statistically significant difference between wild type and disome X and disome XI.

(E) Wild-type (A35954), disome I (A35955), disome V (A35957), disome VIII (A35958), and disome XI (A35959) cells containing a *MRE11-GFP* fusion were analyzed using time-lapse microscopy to analyze cellular morphology and the presence of Mre11-GFP foci in cells. The graphs show the percent of cells that contain one or more Mre11-GFP foci (closed circles) or cumulative cell divisions (closed squares) over time. The duration of each time point was 7.5 minutes. Cell divisions were synchronized so that the time of bud emergence (BE) occurred at zero time point. Wild-type cells treated with 0.1% MMS for 30 minutes prior to the start of imaging were analyzed as a positive control.

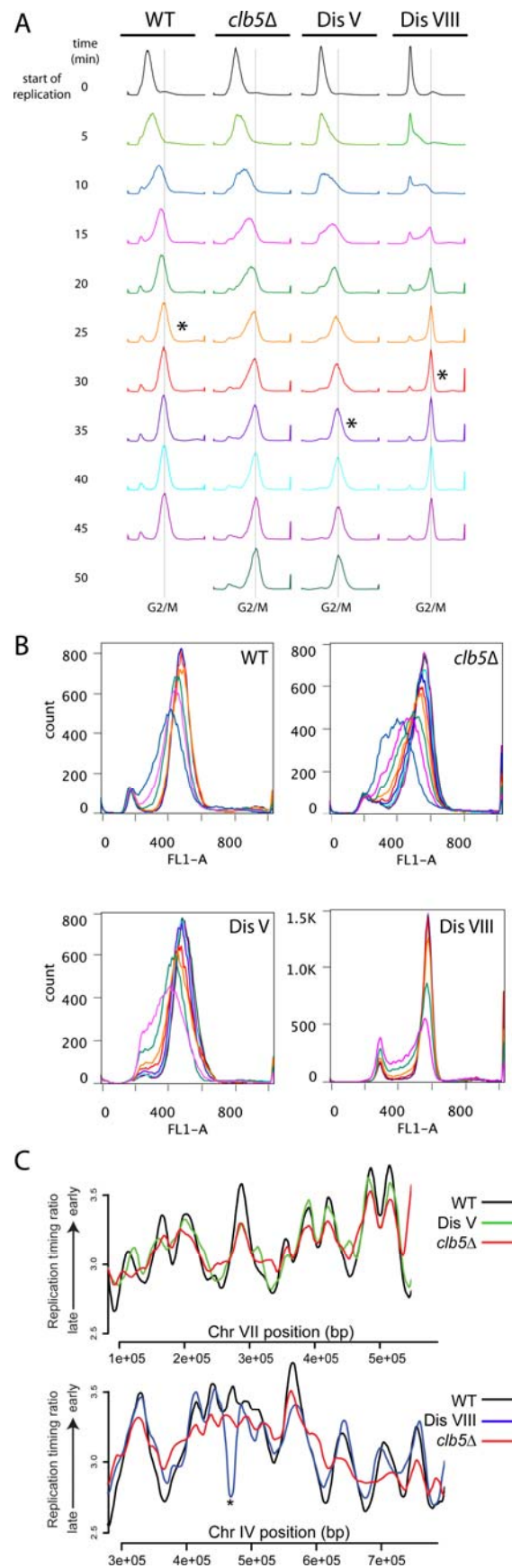


Figure 2: Disome V cells exhibit defects in DNA replication initiation and elongation.

Wild-type (A11311), cells deleted for *CLB5* (A35992), disome V (A28265) and disome VIII (A27036) cells were arrested in G1 with α -factor (5 μ g/ml) for ~165 minutes. Cells were then washed and transferred into medium lacking pheromone. Samples were taken every 5 minutes to determine DNA content by FACS (A, B) and DNA copy number (C). The DNA profiles shown in (A, B) were normalized so that time zero represents the first histogram with noticeable replication. The asterisk in (A) denotes the time point when replication was considered complete. DNA samples from the start of replication to the time point with the asterisk were pooled for each strain for the analysis shown in (C) and Supplemental Figure 2. The graph in (B) shows time points color coded so as to correspond to the histogram profiles from (A) superimposed to illustrate that completion of DNA replication is slow in disome V cells but not disome VIII cells. The replication profiles shown in (C) are the average of three biological replicates and plotted relative to a G1 sample for each strain. The complete replication profiles are shown in Supplemental Figure 2.

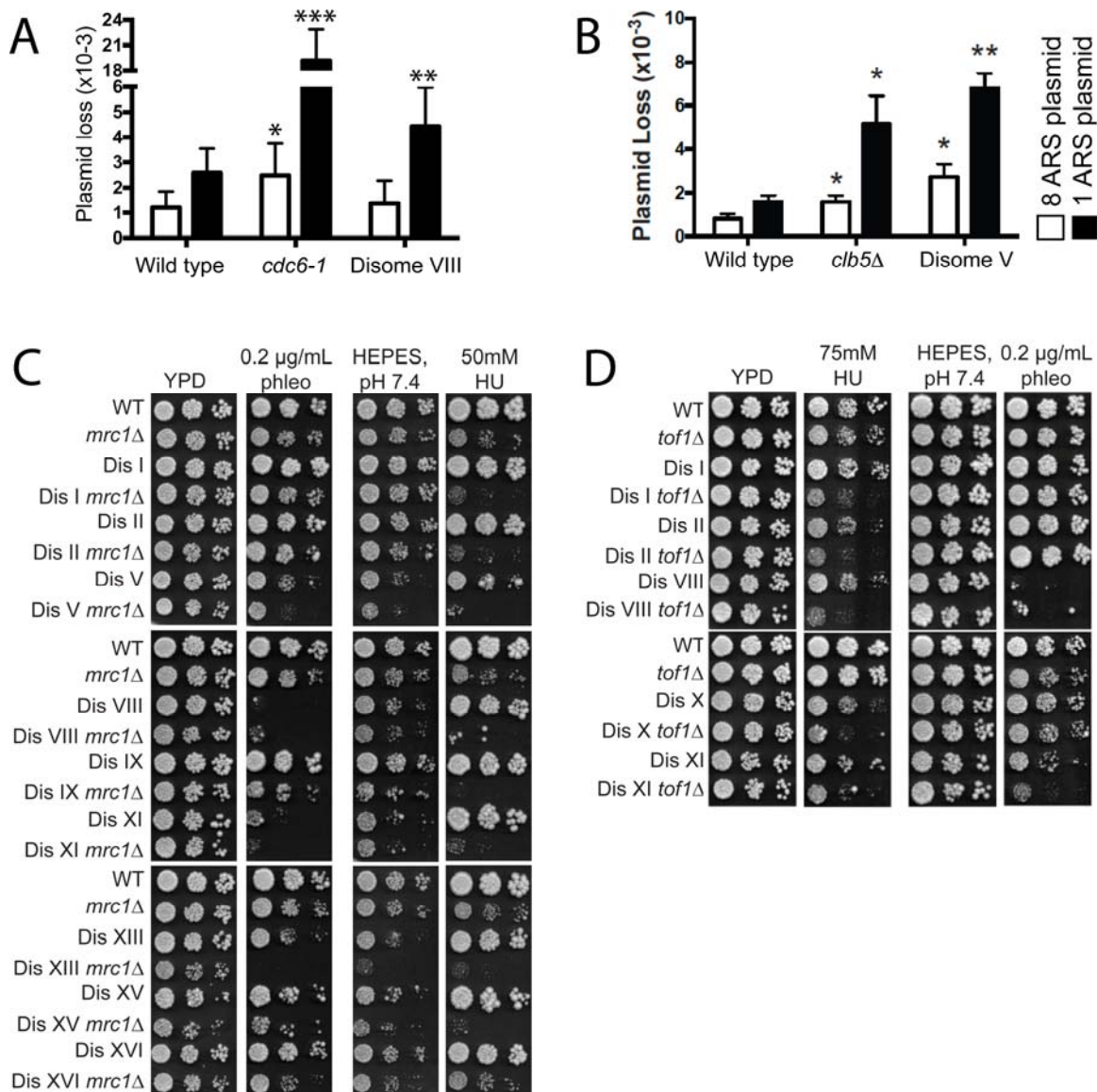


Figure 3: Disome VIII cells exhibit DNA replication initiation defects.

(A) Plasmid loss rate was determined in wild-type (A35934, A35933), *cdc6-1* (A35944, A35943) and disome VIII (A35937, A35938) cells harboring a plasmid bearing either 1 or 8 ARS sequences as described in Materials and Methods. Graphs indicate the mean and standard deviation of at least 12 independent cultures. Statistical tests were performed between the wild-type strain harboring the 8 ARS plasmid and the mutant or disomic strains harboring the 8 ARS plasmid, or between the wild-type strain harboring the 1 ARS plasmid and the mutant or disomic strains harboring the 1 ARS plasmid. * $p < .05$; ** $p < .005$; *** $p < .0005$ (Wilcoxon rank-sum test).

(B) Plasmid loss rate was determined in wild-type (A35934, A35933), *clb5::URA3* (A36737, A36739) and disome V (A36896, A36897) cells harboring a plasmid bearing either 1 or 8 ARS sequences as described in Materials and Methods. Graphs indicate the mean and standard deviation of 3 independent cultures. Statistical tests were performed between the wild-type strain harboring the 8 ARS plasmid and the mutant or

disomic strains harboring the 8 ARS plasmid, or between the wild-type strain harboring the 1 ARS plasmid and the mutant or disomic strains harboring the 1 ARS plasmid. * $p < .05$; ** $p < .005$; *** $p < .0005$ (Wilcoxon rank-sum test).

(C) Ten-fold dilutions of euploid and disomic cells wild-type or mutant for *MRC1* on YEPD plates or YEPD plates + 50mM hydroxyurea or on YEPD+HEPES pH7.4 and YEPD+HEPES pH7.4 + 0.2 μ g/ml phleomycin are shown.

(D) Ten-fold dilutions of euploid and disomes cells wild-type or mutant for *TOF1* on YEPD plates or YEPD plates + 75 mM hydroxyurea or on YEPD+HEPES pH7.4 and YEPD+HEPES pH7.4 + 0.2 μ g/ml phleomycin are shown.

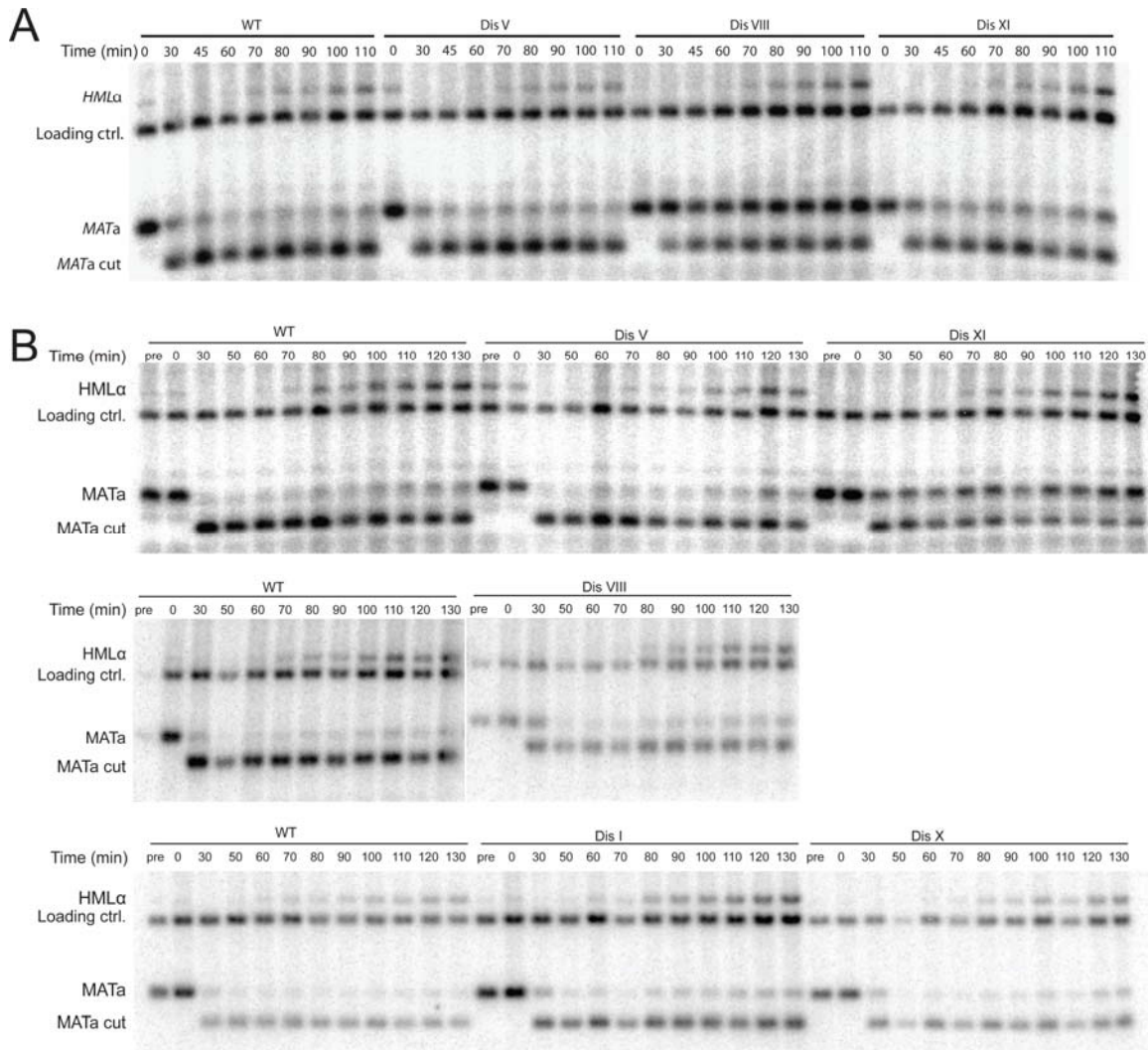


Figure 4: Repair of an HO-induced double strand break occurs normally in disome I, V, VIII, X and XI.

(A) Wild-type (A35884), disome V (HB392), disome VIII (A35886) and disome XI (A35885) cells containing a *GAL-HO* fusion were grown to exponential phase in YEP medium containing 2% lactate. Galactose (2%) was then added ($t=0$) and *MATa* cleavage (*MATa* cut) and repair from the *HMLα* locus (*HMLα*) was analyzed at the indicated times. 40 minutes after *HO* induction, 2% glucose was added to repress *HO* expression. Note that 20 percent of disome V cells had lost the additional chromosome despite continuous selection for both copies of chromosome V (Supplemental Figure 4). We therefore did not keep this strain.

(B) Wild-type (A35884), disome I (A35892), disome V (HB392), disome VIII (A35886), disome X (A35891) and disome XI (A35885) cells containing a *GAL-HO* fusion were grown as in (A) but cells were treated with phleomycin (10μg/mL) in HEPES buffered medium for 1 hour prior to addition of galactose and throughout the duration of the experiment, with the exception of the top panel, where phleomycin was only present in the one hour prior to the addition of galactose.

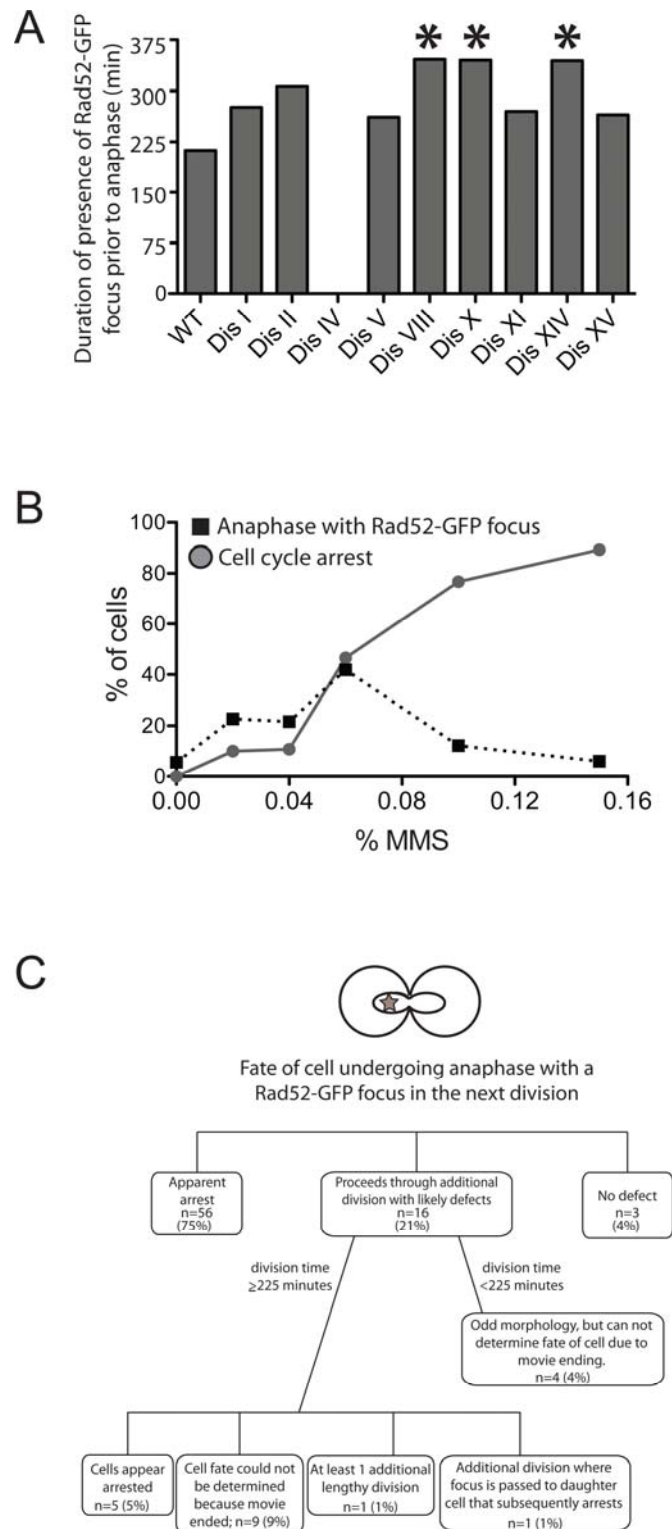


Figure 5: Disomic yeast strains undergo anaphase in the presence of DNA damage.

(A) Time lapse microscopy movies described in Figure 1 were analyzed to determine the amount of time the WT and disomic yeast strains harbored a Rad52-GFP focus before

entering anaphase despite the presence of a Rad52-GFP fusion. WT n=18; Disome I n=23; Disome II n=12; Disome IV not analyzed; Disome V n=14; Disome VIII n=11; Disome X n=10; Disome XI n=9; Disome XIV n=20; Disome XV n=18. Statistical differences between wild-type and disomes were determined by a one way ANOVA of all disomes but disome IV followed by a post-hoc Tukey HSD test of significance. This analysis showed that the difference between wild-type and disomes VIII ($p=0.0174$), X ($p=0.0267$) and XIV ($p=0.0026$) to be statistically significant (indicated with an asterisk). The other differences were not.

(B) Wild-type cells (A24352) were treated with the indicated amounts of MMS and analyzed by time lapse microscopy. The percentage of cells undergoing anaphase in the presence of a Rad52-GFP focus (black squares) or that arrested in metaphase (closed circles) was determined. 0% MMS n=81; 0.02% MMS n=88; 0.04% MMS n=37; 0.06% MMS n=43; 0.08% MMS n=90; 0.1% MMS n=90; 0.15% MMS n=84.

(C) Schematic describing the fate of wild-type cells treated with MMS (data from all concentrations pooled) analyzed in (B) that underwent anaphase in the presence of a Rad52-GFP focus.